Available online at www.sciencedirect.com
ScienceDirect
Trans. Nonferrous Met. Soc. China 24(2014) 3858−3865
Transactions of Nonferrous Metals Society of China
www.tnmsc.cn

Aging behavior and mechanical properties of 6013 aluminum alloy processed by severe plastic deformation

Man-ping LIU[1], Ting-hui JIANG[1], Jun WANG[1], Qiang LIU[1], Zhen-jie WU[1], Ying-da YU[2], Pål C. SKARET[2], Hans J. ROVEN[2,3]

1. School of Materials Science and Engineering, Jiangsu Province Key Laboratory of Materials Tribology, Jiangsu University, Zhenjiang 212013, China;
2. Department of Materials Science and Engineering, Norwegian University of Science and Technology, Trondheim 7491, Norway;
3. Center for Advanced Materials, Qatar University, P.O. Box 2713, Doha, Qatar

Received 17 October 2013; accepted 7 November 2014

Abstract: Structural features, aging behavior, precipitation kinetics and mechanical properties of a 6013 Al–Mg–Si aluminum alloy subjected to equal channel angular pressing (ECAP) at different temperatures were comparatively investigated with that in conventional static aging by quantitative X-ray diffraction (XRD) measurements, differential scanning calorimetry (DSC) and tensile tests. Average grain sizes measured by XRD are in the range of 66−112 nm while the average dislocation density is in the range of 1.20×10^{14}−1.70×10^{14} m^{-2} in the deformed alloy. The DSC analysis reveals that the precipitation kinetics in the deformed alloy is much faster as compared with the peak-aged sample due to the smaller grains and higher dislocation density developed after ECAP. Both the yield strength (YS) and ultimate tensile strength (UTS) are dramatically increased in all the ECAP samples as compared with the undeformed counterparts. The maximum strength appears in the samples ECAP treated at room temperature and the maximum YS is about 1.6 times that of the statically peak-aged sample. The very high strength in the ECAP alloy is suggested to be related to the grain size strengthening and dislocation strengthening, as well as the precipitation strengthening contributing from the dynamic precipitation during ECAP.

Key words: Al−Mg−Si aluminum alloy; severe plastic deformation; equal-channel angular pressing; aging behavior; precipitation kinetics; mechanical properties; strengthening mechanisms

1 Introduction

Over the last two decades, bulk materials with ultrafine-grained (UFG) alloys processed by severe plastic deformation (SPD) have attracted widespread interest in scientific and technological communities [1]. One of the major SPD methods is equal channel angular pressing (ECAP), which has been widely used to fabricate UFG materials [2]. ECAP processing is an attractive procedure for many advanced structural and functional applications as it allows enhancing significant properties of commonly used metals and alloys [1−3]. Although outstanding progress has been made in this area in recent years, the relationships between theory-based structure and property in SPD metals are not yet fully understood [4].

Al−Mg−Si alloys have been extensively studied due to their superior yield strength (YS) and ultimate tensile strength (UTS) obtained by precipitation hardening [5−8]. The formation of metastable phases influences its mechanical properties. It is important to understand the precipitation sequence of the metastable phases and their kinetics for achieving the superior mechanical properties in Al−Mg−Si alloys. The precipitation sequences of this alloy were reported in Ref. [9] as follows: $\alpha\rightarrow$GP

Foundation item: Project (BK2012715) supported by the Basic Research Program (Natural Science Foundation) of Jiangsu Province, China; Project (14KJA430002) supported by the Key University Science Research Project of Jiangsu Province, China; Project (50971087) supported by the National Natural Science Foundation of China; Projects (11JDG070, 11JDG140) supported by the Senior Talent Research Foundation of Jiangsu University, China; Project (hsm1301) supported by the Foundation of the Jiangsu Province Key Laboratory of High-end Structural Materials, China; Project (Kjsmcx2011004) supported by the Foundation of the Jiangsu Province Key Laboratory of Materials Tribology, China

Corresponding author: Man-ping LIU; Tel: +86-511-88780192; E-mail: manping-liu@263.net; manpingliu@ujs.edu.cn

DOI: 10.1016/S1003-6326(14)63543-3

zones→β''→β'→β, where α is the supersaturated solid solution; GP zones are generally spherical clusters with unknown structure [10]; β'' precipitates are fine needle-shaped zones with monoclinic structure and are generally present in Al alloys aged to the maximum hardness; β' is rod-shaped precipitates with hexagonal structure and is found in the overaged specimens; β (Mg_2Si) is an equilibrium phase in the precipitation sequence.

Precipitation kinetics in Al alloys has been studied by numerous investigators by differential scanning calorimetry (DSC) [10−12]. Several analytical schemes were used to determine the kinetic parameters from the scan rate dependence of peaks observed in DSC curves [11]. The study on precipitation kinetics and microstructural characterization of heat treatable Al-based bulk alloys is abundant but it is very scarce for ultrafine-grained Al alloys. The knowledge of kinetics of precipitate formation and its dissolution in ultrafine-grained Al−Mg−Si alloys is very essential to understand the thermal stability of its microstructures as well as the role of strengthening mechanisms.

In the present work, a commercial 6013 Al−Mg−Si−Cu aluminum alloy was subjected to ECAP at different temperatures. The structural features, aging behavior, precipitation kinetics in the ECAP alloy were compared with that in conventional static aging by DSC and quantitative X-ray diffraction (XRD) measurements. Mechanical properties were comparatively investigated and the strengthening mechanisms involved in the deformed alloy were interpreted.

2 Experimental

Commercially extruded rods with a diameter of 25 mm of the 6013 Al alloy were purchased from ALCOA in the peak-aged temper (T6-condition). The composition of the alloy is given in Table 1. Square billets cut from the as-received rods were first solution-treated (ST) at 560 °C for 2 h, followed by quenching in water, then immediately processed by ECAP (1 to 4 passes) with route Bc. The ECAP was performed at room temperature (RT), 110 °C and 170 °C, respectively. The ECAP die had a channel intersection angle Φ=90°, arc of curvature Ψ=20.6° and the billet dimensions were 19.5 mm×19.5 mm×100 mm [13]. For comparison, conventional static aging was conducted in the as-received materials which were first solution-treated at 560 °C for 2 h, followed by water quenching, then immediately aged at 191 °C for 10 min to 25 h.

Table 1 Composition of 6013 Al alloy (mass fraction, %)

Mg	Si	Cu	Mn	Fe
0.8−1.2	0.6−1.0	0.6−1.1	0.2−0.8	≤0.5
Zn	Ti	Cr	Al	
≤0.25	≤0.1	≤0.1	Bal.	

To investigate the influence of ECAP on phase precipitation during aging, samples of the processed alloy were also subjected to DSC analyses. Specimens were cut from bulk samples and cleaned with ultrasonic wave. The final mass of each DSC sample was about 30 mg. The sample for DSC testing was equilibrated at 20 °C and then heated to 500 °C with a heating rate of 10 °C/min under an argon atmosphere. The structural characterization was performed by quantitative XRD. Quantitative XRD measurements were performed with a D/max–2500PC diffractometer using Cu K_α radiation at 40 kV and 30 mA. Vickers microhardness (HV) was measured using a HV−1000 microindentation tester under a load of 1.96 N for 20 s. Each hardness was averaged over at least 5 measurements. Tensile tests were precisely performed with a WDW−10 computer controlled electronic universal testing machine at room temperature at a strain rate of 10^{-4} s^{-1} operating with a constant displacement of the specimen grips. The yield strength (YS, $\sigma_{0.2}$), ultimate tensile strength (UTS, σ_{UTS}) and elongation (δ) were determined from the tests not less than three samples. The standard deviation of the tensile tests did not exceed 5%.

3 Results

3.1 Structural features

The XRD peaks of the materials processed by ECAP at different temperatures and the quantitative XRD measurements are shown in Table 2 and Fig. 1, respectively. The X-ray measurements demonstrate that the temperature of ECAP strongly influences the subgrain size of the investigated alloy. The size of coherent domains, D_{XRD}, increases tremendously from 66 to 112 nm as the temperature increases from RT to 170 °C (see Table 2). It should be noted that the grain sizes (d) in the ECAP alloy measured by the dark field images are often larger than the D_{XRD} obtained by the XRD. The emergence of this difference is because the XRD process determines the size of the coherent diffraction domains and this includes both the subgrains and the dislocation cells [14−17]. The microstrain, $\langle\varepsilon^2\rangle^{1/2}$, increases significantly from 0.092% to 0.107% as the temperature increases from RT to 170 °C (see Table 2). For the materials subjected to equal channel angular pressing, the dislocation density is proportional to microstrain and inversely proportional to grain size [14]. Using the experimentally obtained values (see Table 2) of D_{XRD} and $\langle\varepsilon^2\rangle^{1/2}$, the dislocation density in the ECAP treated alloy was calculated by the formula employed in Refs. [16,17]:

Table 2 Microstructural characteristics of ECAP alloy determined by quantitative XRD

State	D_{XRD}/nm	$\langle\varepsilon^2\rangle^{1/2}$/%	$\rho/10^{14}m^{-2}$
ST+ECAP treated at RT	66	0.092	1.70
ST+ECAP treated at 110 °C	74	0.093	1.53
ST+ECAP treated at 170 °C	112	0.107	1.20

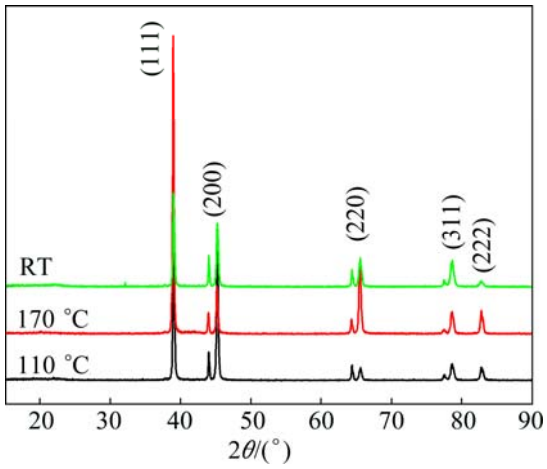

Fig. 1 XRD patterns of 6013 Al alloy after ECAP at different temperatures

$$\rho = 2\sqrt{3}\frac{\langle\varepsilon^2\rangle^{1/2}}{D_{XRD}b} \quad (1)$$

where $b=\sqrt{2}\,a\,/2$ is the magnitude of the Burgers vector and a (0.4049 nm) is the lattice parameter of Al. As shown in Table 2, the calculated dislocation density of the alloy processed by ECAP at RT is larger than the others. All above measurements indicate that the grain sizes, microstrains and dislocation densities of the ECAP alloy are strongly influenced by the temperature of process.

3.2 Precipitation kinetics

The main aim of the DSC analysis is the evaluation of precipitation kinetics in 6013 alloy in some temperature ranges. Thus, with the purpose, samples processed by ECAP at different temperatures were analyzed by DSC equipment. Figure 2 shows the DSC curves for the alloy peak-aged at 191 °C for 4 h and ECAP treated at different temperatures (RT, 110 °C and 170 °C) with the heating rate of 10 °C/min. As shown in Fig. 2, the endothermic peaks are distinguished from the exothermic peaks by using symbol prime ‘’ and the reaction peaks of the solute rich clusters, GP-zones, β'',

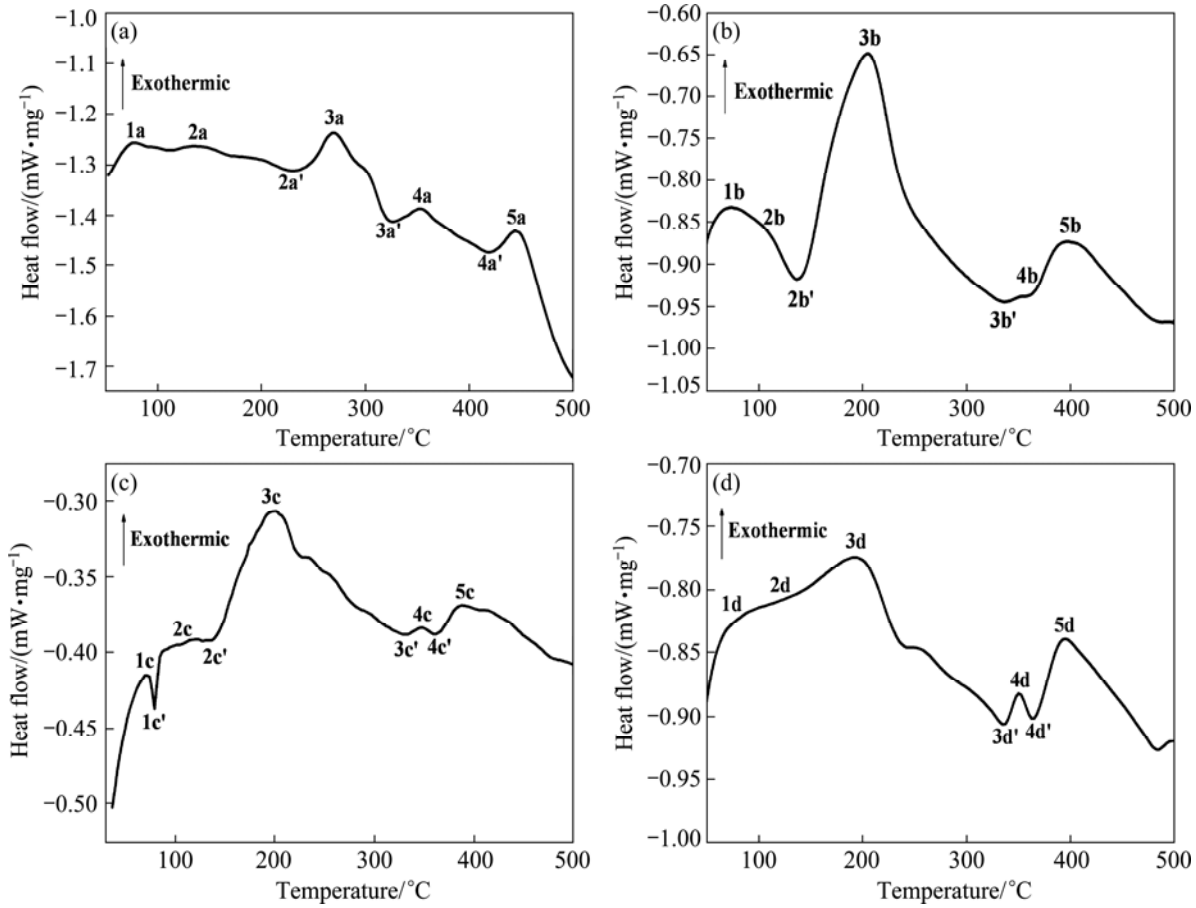

Fig. 2 DSC plots for heat flow of precipitate reactions of peak-aged and ECAP treated 6013 Al alloy samples: (a) Aged at 191 °C for 4 h; (b) ECAP treated at RT; (c) ECAP treated at 110 °C; (d) ECAP treated at 170 °C

β' and β are indicated with numbers 1, 2, 3, 4 and 5, respectively. The DSC curve of the peak-aged alloy in Fig. 2(a) shows five exothermic peaks (upward peaks) and three endothermic peaks (downward peaks). The exothermic reaction peak 1a at temperature of 50−80 °C represents the formation of solute-rich clusters. The formation of GP-zones or Si−Mg-vacancy clusters (peak 2a) is observed at temperature of 120−140 °C. The endothermic peak 2a′ (140−240 °C) may be attributed to the dissolution of the preformed clusters/GP zones. The formation of coherent precipitate β'' and incoherent precipitate β' is observed at temperature of 240−270 °C (peak 3a) and 320−360 °C (peak 4a), respectively. The endothermic peak 3a′ (270−320 °C) is probably caused by the dissolution of the precipitate β'' and the dissolution of β' is the endothermic peak 4a′ (360−420 °C). The formation of equilibrium β occurred at 420−500 °C (peak 5a). The reaction peaks of the precipitation kinetics in the peak-aged alloy are in accordance with the published literatures on similar alloys [18−20].

For the Al 6013 alloy ECAP treated at different temperatures (see Figs. 2(b), (c) and (d)), the DSC peaks corresponding to formation and dissolution of precipitates were shifted to left compared with that of its aged alloy. This is because of heavy deformation of Al alloys during ECAP which accelerates aging kinetics of precipitate formation and dissolution [18]. The first exothermic peaks (1b, 1c, 1d), the second exothermic peaks (2b, 2c, 2d) and the fourth exothermic peaks (4b, 4c, 4d) of the ECAP treated samples are about 20 °C lower than those (1a, 2a, 4a) of the peak-aged sample. While the fifth exothermic peaks (5b, 5c, 5d) for the formation of equilibrium β in the ECAP treated samples are about 50 °C lower than that (5a) of the peak-aged sample. In particular, the exothermic peaks (3b, 3c, 3d) responsible for the formation of coherent precipitate β'' in the ECAP treated samples are much lower than that (3a) of the peak-aged sample and the difference is about 80 °C. At the same time, the endothermic peaks (3b′, 3c′, 3d′) of the ECAP treated samples are observed at temperature of 200−350 °C and the range gaps are about 150 °C. While the range gap of the endothermic peak 3a′ (270−320 °C) in the peak-aged sample is only about 50 °C. These data indicate that the endotherm gaps (about 150 °C) caused by the dissolution of the precipitate β'' in the ECAP treated samples are much broader than those (about 50 °C) in the peak-aged sample.

It is well known that, the hardening in Al−Mg−Si alloys is mainly caused by precipitation of β'' phase. The above DSC analysis shows that the β'' precipitation peak temperatures clearly decrease in all the three ECAP treated samples. These results indicate that the aging kinetics of the β'' precipitate formation has been accelerated and the activation energy for the β'' formation decreased when ECAP was carried out. There are two possible reasons for the rapider kinetics and lower activation energy for the β'' formation in the ECAP treated alloy. Smaller grains developed after ECAP (see Table 2) provide an excess free energy associated with higher volume fraction of the grain boundaries, which reduces the activation energy during the formation of the precipitates [18]. A high density of dislocations induced by ECAP (see Table 2) makes the precipitates easier to nucleate around or at dislocations and the precipitation in the ECAP treated alloy is most likely a dislocation-assisted process [18,21].

3.3 Mechanical properties

The microhardness of the static aged 6013 alloy was substantially influenced by the aging time at 191°C (see Fig. 3). It can be seen that small fluctuations in microhardness exist in the very beginning of aging (0−10 min). In this aging time, the precipitates in the Al matrix are the fully coherent GP zones, which have a relatively small contribution to the hardness of the alloy. The hardness of the alloy starts to increase after being aged for about 1 h. The hardness reaches its peak value at about 4 h as the needle-shaped β'' precipitates have the maximum density. The hardness starts to decrease with the appearance of the β' and β precipitates. The static aging behavior seems to be influenced by the aging time in the usual manner. However, two hardness peaks were observed. The first peak hardness (peak I, 1.09 GPa) occurred around 4 h aging time and the second peak (peak II, 1.04 GPa) appeared at around 10 h. At the final stage of aging, the hardness decreased gradually as a result of over-aging. As reported in our previous work in a commercial 6063 Al−Mg−Si alloy [21], the second aging peak in such alloys may be ascribed to the formation of fine metastable β' precipitates during the

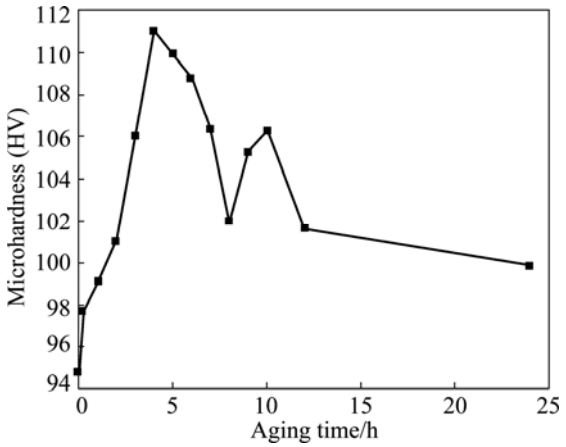

Fig. 3 Conventional (static) aging curve of as-solutionized alloy at 191 °C

transition from β'' to β' phase. During this period, the β' metastable precipitates seemed to nucleate and grow up at the expense of fine and uniformly dispersed β'' precipitates. These metastable phases formed between the two hardening peaks, probably kept their semi-coherence with the matrix and are believed to be effectively resistant to the movement of dislocations, thus have certain strengthening effects [21].

The results of tensile tests of the samples in the alloy both before and after ECAP are presented in Table 3 and Fig. 4. Figure 4 shows the typical engineering stress–strain curves of the aged and deformed samples and all the mechanical data are listed in Table 3. As shown in Table 3 and Fig. 4(a), the strength values of the statically aged samples exhibit similar tendency of the microhardness values to that in Fig. 3. Obviously, the strength of the alloy in solution-treated state is the lowest and the UTS and YS are 213 MPa and 102 MPa, respectively. The YS increases to 203 MPa when the aging time is 1 h and this time is believed in underaging period (see Fig. 3). The peak strength appears around at 4 h aging time and the peak UTS and YS are 310 MPa and 258 MPa, respectively. As the aging time exceeds the peak time (4 h) the strength is decreased gradually due to the fact that the alloy is entered to the overaging state. The YS decreases to 204 MPa as the alloy is overaged for 24 h.

Table 3 Mechanical properties of alloy

State	$\sigma_{0.2}$/MPa	σ_{UTS}/MPa	δ/%
ST	102	213	20
ST+(191°C, 1 h)	203	269	19
ST+(191°C, 4 h)	258	310	16
ST+(191°C, 24 h)	204	286	14
ST+ECAP at RT	404	459	18
ST+ECAP at 110 °C	402	452	22
ST+ECAP at 170 °C	316	356	20

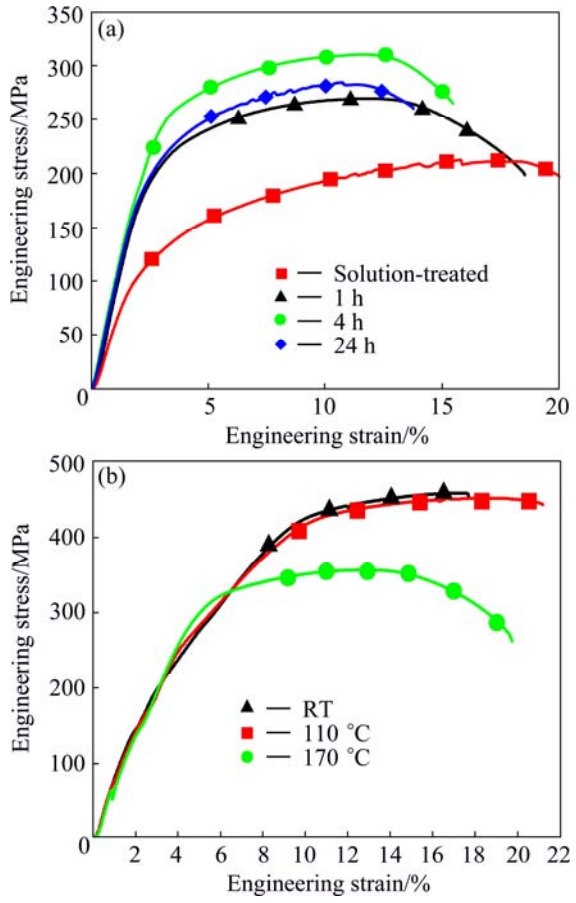

Fig. 4 Engineering stress−strain curves of 6013 Al alloy: (a) Statically aged at 191 °C for different aging time; (b) ECAP treated at different temperatures

Interestingly, both the UTS and YS increase dramatically after ECAP for all samples as compared with the undeformed counterparts (see Table 3 and Fig. 4(b)). The yield strength ranging from 316 to 404 MPa in the deformed alloy is about three to four times that of the solution-treated samples and the ultimate tensile strength is approximately two to three times that obtained in the same undeformed alloy. For example, the YS values of sample ECAP treated at RT, 110 °C and 170 °C are 404, 402 and 316 MPa, respectively. These values are about 4.0, 3.9 and 3.1 times that of the ST sample (102 MPa). At the same time, all the strength values of the ECAP treated samples are considerably higher than those of the statically peak aged sample. Compared with the YS (258 MPa) of the statically peak-aged sample, the YS values of the samples ECAP treated at RT, 110 °C and 170 °C are increased by 57%, 56% and 22%, respectively. While the UTS values of the ECAP treated samples at RT, 110 °C and 170 °C are about 149, 142 and 46 MPa higher than that (310 MPa) of the static peak-aging.

The above data indicate that the ECAP process results in a significant increase in strength compared with the peak strength of the static aging alloy. As seen in Table 2 measured by XRD in the ECAP treated samples, the grain sizes are achieved in the range of 66−112 nm and the average dislocation density is as high as 10^{14} m^{-2}. These XRD results suggest that the higher strength achieved after ECAP may be attributed to grain refinement strengthening and dislocation strengthening. Furthermore, the DSC analysis (see Fig. 2) presents that heavy deformation of Al alloys during ECAP has accelerated the aging kinetics of precipitate formation and dissolution. In addition, our previous work has provided experimental evident of the dynamic precipitation of the β'' precipitates in a commercial 6063 Al−Mg−Si alloy during ECAP [21]. Therefore, it is reasonable to believe that the dynamic precipitation

during ECAP in the 6013 alloy also plays an important role in the strengthening.

4 Discussion

The tensile tests revealed that the mechanical properties of deformed 6013Al alloy are dramatically higher than those of their undeformed counterparts. The strengthening mechanisms involved in the deformed alloy may include solid solution strengthening, grain size strengthening, dislocation strengthening and precipitation strengthening. Contributions from different strengthening mechanisms are often taken to be additive assuming that they act independently, and the total strength of the present nanostructured Al alloy could be estimated as [4,22−27]

$$\sigma_{0.2}=\sigma_0+\sigma_{ss}+\sigma_{gs}+\sigma_p+\sigma_{preci} \quad (2)$$

where $\sigma_{0.2}$ is the total yield strength (YS_{calc}); σ_0 is the Peierls or friction stress; σ_{ss} is solid solution strengthening; σ_{gs} is grain size strengthening; σ_p is dislocation strengthening; σ_{preci} is the precipitation strengthening contributing from the dynamic precipitation of the 6013 Al alloy during ECAP. The value of friction stress for the ECAP treated alloy is taken as that of pure Al (about 20 MPa) considering that other strengthening mechanisms were found to increase the friction stress in the Al alloy [27,28].

The grain size strengthening is generally described by a Hall–Petch equation [29]. As shown in Fig. 1 and Table 2, the grain size increases tremendously with the temperature of ECAP in the samples. The smaller grain size indicates that more grain or sub-grain boundaries are contributed to the strengthening. The contribution of the grain size strengthening (σ_{gs}) is described by the equation based on the Hall–Petch equation [27,29]:

$$\sigma_{gs}=Kd^{-1/2} \quad (3)$$

where K is a positive constant of yielding, and d is the grain size. It was reported that K is about 0.040 MPa·m$^{1/2}$ for high purity Al, while for less-pure Al or for Al−(2−3)Mg, higher K slopes of about 0.07−0.17 MPa·m$^{1/2}$ have been proposed [28,30]. Such an increase of K-slope was related to the presence of other strengthening mechanisms contributing to the total strength of the alloy since the Hall−Petch relation was plotted directly using the experimentally measured yield strength values [27]. Indeed, estimation of the K-slope for the original mechanism of grain boundary dislocation pile-up (by subtracting all other present strengthening contributions from the total yield strength) led to K=0.06−0.09 MPa·m$^{1/2}$, coinciding with that estimated in pure nanocrystalline Al [27,31]. Therefore, the value of K in the present ECAP treated Al alloy is taken as 0.040 MPa·m$^{1/2}$ as that of high purity Al [30]. According to Eq. (3) and the values of grain size in Table 2, the calculated values of the grain size strengthening are about 155, 147 and 119 MPa for sample ECAP treated at RT, 110 °C and 170 °C, respectively (see Table 4).

Both the quantitative XRD measurements (see Table 2) and the tensile tests (see Table 3, Fig. 4(b)) suggest that dislocation strengthening may contribute significantly to the strength enhancement. The excess dislocations within grains and near grain or sub-grain boundaries make dislocation glide more difficult [29]. As shown in Table 2, the dislocation density increases significantly with decreasing temperature of process, which is consistent with the significant increase of hardness and strength in the ECAP treated samples (see Table 3, Fig. 4). The contribution of the dislocation strengthening (σ_p) is usually calculated by the Taylor equation [28]:

$$\sigma_p=\alpha MGb\rho^{1/2} \quad (4)$$

where α is a constant (α=0.33); G is the shear modulus (26 GPa); b is the length of the Burgers vector of dislocations (b=0.286 nm), and M is the Taylor factor (M=3). According to Eq. (4) and the values of the dislocation density in Table 1, the calculated values of the dislocation strengthening are about 96, 91 and 81 MPa for samples ECAP treated at RT, 110 °C and 170 °C, respectively (see Table 4).

As such, the total yield strength contributing from the dislocation strengthening and the grain size strengthening are added up by

$$\sigma_{0.2}=\sigma_0+\sigma_{gs}+\sigma_p \quad (5)$$

The calculated YS_{calc} values from Eq. (5) are 271, 258 and 220 MPa for samples ECAP treated at RT, 110 °C and 170 °C, respectively (see Table 4). These values are much smaller than the experimental values 404, 402 and 316 MPa for samples ECAP treated at RT, 110 °C and 170 °C, respectively (see Table 3 and Table 4).

The above calculations indicate that the conventional strengthening mechanisms from the dislocation strengthening and the grain size strengthening only provide about 67% of the total strength. This means that additionally strengthening mechanisms should be accounted another about 33% for the total strength in the present ECAP treated alloy.

Table 4 Contribution of strengthening mechanisms to strength of ECAP alloy

State	YS_{exp}/ MPa	σ_{gs}/ MPa	σ_p/ MPa	$(\sigma_0+\sigma_{gs}+\sigma_p)$/ MPa	σ_{preci}/ MPa
ST+ECAP at RT	404	155	96	271	133
ST+ECAP at 110 °C	402	147	91	258	144
ST+ECAP at 170 °C	316	119	81	220	96

These additionally strengthening mechanisms may primarily be related to the contribution from the dynamic precipitation of the Al 6013 alloy during ECAP [21]. Therefore, the values of the dynamic precipitation strengthening are about 133, 144 and 96 MPa for samples ECAP treated at RT, 110 °C and 170 °C, respectively (see Table 4).

5 Conclusions

1) The grain sizes and dislocation densities of the ECAP treated alloy are strongly influenced by the temperature of process. Average grain sizes measured by XRD are in the range of 66−112 nm while the average dislocation density is in the range of 1.20×10^{14}–1.70×10^{14} m^{-2} in the deformed alloy.

2) Five exothermic peaks and three endothermic peaks are observed by the DSC curve in the peak-aged alloy. These reaction peaks are in accordance with the published literatures on similar alloys.

3) The DSC analysis reveals that the peak temperatures corresponding to formation and dissolution of precipitates are clearly decreased in the ECAP treated samples compared with the peak-aged sample. The precipitation in the ECAP treated alloy is most likely a dislocation-assisted process.

4) Two hardness peaks are observed in the 6013 Al alloy statically aged at 191°C. The needle-shaped β'' precipitates are believed to be responsible for the first peak in around 4 h aging time. The second peak in around 10 h aging time may be ascribed to the formation of fine metastable β' precipitates during the transition from β'' to β' phase.

5) Both the UTS and YS are dramatically increased in all the ECAP samples compared with undeformed counterparts. The maximum strength appears in the sample ECAP treated at room temperature.

6) The strengthening mechanisms contributing to the very high strength may depend not only on the conventional mechanisms of grain size strengthening and dislocation strengthening, but also on the mechanism related to the contribution from the dynamic precipitation of the Al 6013 alloy during ECAP.

References

[1] HAN W Z, LI S X, WU S D. Deformation mechanisms of single crystals and bicrystals subjected to equal-channel angular pressing—Review [J]. Mater Sci Forum, 2010, 633: 511−525.

[2] VALIEV R Z, ISLAMGLIEV R K, ALEXANDROV I V. Bulk nanostructured materials from severe plastic deformation [J]. Prog Mater Sci, 2000, 45(2): 103−189.

[3] VALIEV R Z, ESTRIN Y, HORITA Z. Producing bulk ultrafine-grained materials by severe plastic deformation [J]. JOM, 2006, 58(4): 33−39.

[4] LIDDICOAT P V, LIAO X Z, ZHAO Y. Nanostructural hierarchy increases the strength of aluminium alloys [J]. Nature Commun, 2010, 1: 63-1−63-7.

[5] AN X H, WU S D, ZHANG Z F. Evolution of microstructural homogeneity in copper processed by high-pressure torsion [J]. Scripta Mater, 2010, 63(5): 560−563.

[6] VALIEV R Z, KORZNIKOV A V, ALEXANDROV I V. Nanomaterials produced by severe plastic deformation: An introduction [J]. Ann Chim-Sci Mat, 2002, 27 (3): 1−2.

[7] CHEN Jiang-hua, LIU Chun-hui. Microstructure evolution of precipitates in AlMgSi(Cu) alloys [J]. The Chinese Journal of Nonferrous Metals, 2011, 21(10): 2352−2360. (in Chinese)

[8] LIU Hong, ZHAO Gang, LIU Chun-ming, ZUO Liang. Effects of different tempers on precipitation hardening of 6000 series aluminium alloys [J]. Transactions of Nonferrous Metals Society of China, 2007, 17(1): 122−127.

[9] WEATHERLY G C, PEROVIC A, PEROVIC D D. The precipitation of the *Q* phase in an AA6111 alloy [J]. Metall Mater Trans A, 2001, 32(2): 213−218.

[10] ESMARILI S, WANG X, LLOYD D J. On the precipitation-hardening behavior of the Al−Mg−Si−Cu alloy AA6111 [J]. Metall Mater Trans A, 2003, 34(13): 751−763.

[11] FANG X, SONG M, LI K. Precipitation sequence of an aged Al−Mg−Si alloy [J]. J Min Metall B, 2010, 46 (2): 171−180.

[12] GHOSH K S, GAO N. Determination of kinetic parameters from calorimetric study of solid state reactions in 7150 Al−Zn−Mg alloy [J]. Transactions of Nonferrous Metals Society of China, 2011, 21(6): 1199−1209.

[13] WERENSKIOLD J C, ROVEN H J. Microstructure and texture evolution during ECAP of an AlMgSi alloy: Observations, mechanisms and modeling [J]. Mater Sci Eng A, 2005, 410: 174−177.

[14] UNGÁR T. Characterization of nanocrystalline materials by X-ray line profile analysis [J]. J Mater Sci, 2007, 42(5): 1584−1593.

[15] ZHU Y T, LIAO X Z, WU X L, NARAYAN J. Grain size effect on deformation twinning and detwinning [J]. J Mater Sci, 2013, 48(13): 4467−4475.

[16] VALIEV R Z, MURASHKIN M Y, GANEEV A V. Superstrength of nanostructured metals and alloys produced by severe plastic deformation [J]. Phys Metals Metallogr, 2012, 113(13): 1193−1201.

[17] ZHILYAEV A P, LANGDON T G. Using high-pressure torsion for metal processing: Fundamentals and applications [J]. Prog Mater Sci, 2008, 53(6): 893−979.

[18] PANIGRAHI S K, JAYAGANTHAN R, PANCHOLI V, GUPTA M. A DSC study on the precipitation kinetics of cryorolled Al 6063 alloy [J]. Mater Chem Phys, 2010, 122: 188−193.

[19] KIM W J, WANG J Y. Microstructure of the post-ECAP aging processed 6061 Al alloys [J]. Mater Sci Eng A, 2007, 464: 23−27.

[20] VEDANI M, ANGELLA G, BASSANI P, RIPAMONTI D, TUISSI A. DSC analysis of strengthening precipitates in ultrafine Al−Mg−Si alloys [J]. J Therm Anal Calorim, 2007, 87: 277−284.

[21] ROVEN H J, LIU M P, WERENSKIOLD J C. Dynamic precipitation during severe plastic deformation of an Al−Mg−Si aluminium alloy [J]. Mater Sci Eng A, 2008, 483−484: 54−58.

[22] HU L J, ZHAO S J. The effect of nanostructural hierarchy on the mechanical properties of aluminium alloys during deformation processes [J]. J Mater Sci, 2012, 47(19): 6872−6881.

[23] SIMAR A, BRECHET Y, MEESTER B D, DENQUIN A, GALLAIS C, PARDOEN T. Integrated modeling of friction stir welding of 6xxx series Al alloys: Process, microstructure and properties [J]. Prog Mater Sci, 2012, 57: 95−183.

[24] LU L, CHEN X, HUANG X. Revealing the maximum strength in nanotwinned copper [J]. Science, 2009, 323(5914): 607−610.

[25] LIU M P, ROVEN H J, LIU X T, MURASHKIN M, VALIEV R Z, UNGÁR T, BALOGH L. Special nanostructures in Al−Mg alloys subjected to high pressure torsion [J]. Transactions of Nonferrous Metals Society of China, 2010, 20 (11): 2051−2056.

[26] LIU M P, ROVEN H J, MURASHKIN M, VALIEV R Z. Structural characterization by high-resolution electron microscopy of an Al−Mg alloy processed by high-pressure torsion [J]. Mater Sci Eng A, 2009, 503: 122−125.

[27] SABIROV I, MURASHKIN M Y, VALIEV R Z. Nanostructured aluminium alloys produced by severe plastic deformation: New horizons in development [J]. Mater Sci Eng A, 2013, 506: 1−24.

[28] GUBICZA J, CHINH N Q, KRÁLLICS G. Microstructure of ultrafine-grained fcc metals produced by severe plastic deformation [J]. Curr Appl Phys, 2006, 6(2): 194−199.

[29] ZHAO Y H, LIAO X Z, JIN Z. Microstructures and mechanical properties of ultrafine grained 7075 Al alloy processed by ECAP and their evolutions during annealing [J]. Acta Mater, 2004, 52(15): 4589−4599.

[30] GUTIERREZ-URRUTIA I, MUNOZ-MORRIS M A, MORRIS D G. Recovery of deformation substructure and coarsening of particles on annealing severely plastically deformed Al−Mg−Si alloy and analysis of strengthening mechanisms [J]. J Mater Res, 2006, 21(2): 329−342.

[31] SHANMUGASUNDARAM T, HEILMAIER M, MURTY B S. On the Hall–Petch relationship in a nanostructured Al−Cu alloy [J]. Mater Sci Eng A, 2010, 527(29): 7821−7825.

大塑性变形 6013 铝合金的时效特性与力学性能

刘满平[1]，蒋婷慧[1]，王 俊[1]，刘 强[1]，吴振杰[1]，Ying-da YU[2], Pål C. SKARET[2], Hans J. ROVEN[2,3]

1. 江苏大学 材料科学与工程学院，江苏省材料摩擦学重点实验室，镇江 212013；
2. Department of Materials Science and Engineering, Norwegian University of Science and Technology, Trondheim 7491, Norway;
3. Center for Advanced Materials, Qatar University, P.O. Box 2713, Doha, Qatar

摘 要：利用 X 射线衍射分析(XRD)、差示扫描量热法(DSC)和拉伸试验，研究不同温度等通道转角挤压 (ECAP)和常规静态时效处理后 6013 Al−Mg−Si 铝合金的微观结构、时效行为、析出动力学以及力学性能。XRD 测得的 ECAP 变形后合金的平均晶粒尺寸在 66~112 nm 范围内，平均位错密度在 1.20×10^{14}~1.70×10^{14} m^{-2} 范围内。DSC 分析表明，由于 ECAP 后试样比常规时效处理试样拥有更细小的晶粒和更高的位错密度，因此，ECAP 变形后合金的析出动力学更快。与未变形合金相比，ECAP 后试样的屈服强度和抗拉强度都得到了显著提高。室温 ECAP 后试样的强度达到最大，其屈服强度是静态峰时效屈服强度的 1.6 倍。细晶强化、位错强化以及由于 ECAP 过程中的动态析出而产生的析出相强化，是 ECAP 合金获得高强度的几种主要强化机制。

关键词：Al−Mg−Si 铝合金；大塑性变形；等通道转角挤压；时效特性；析出动力学；力学性能；强化机制

(Edited by Xiang-qun LI)